2024

Evolution of Efimov States

Sebastian M. Dawid
University of Washington

Md Habib E. Islam
Old Dominion University, m2islam@odu.edu

Raúl A. Briceño
University of California - Berkeley

Andrew W. Jackura
William & Mary

Original Publication Citation

Dawid, S. M., Islam, M. H. E., Briceño, R. A., & Jackura, A. W. (2024). Evolution of Efimov states. *Physical Review A*, *109*(4), 1-13, Article 043325. https://doi.org/10.1103/PhysRevA.109.043325

Evolution of Efimov states

Sebastian M. Dawid,[1,*] Md Habib E. Islam,[2,3,†] Raúl A. Briceño,[4,5,‡] and Andrew W. Jackura[4,5,6,§]

[1]*Physics Department, University of Washington, Seattle, Washington 98195-1560, USA*
[2]*Department of Physics, Old Dominion University, Norfolk, Virginia 23529, USA*
[3]*Thomas Jefferson National Accelerator Facility, 12000 Jefferson Avenue, Newport News, Virginia 23606, USA*
[4]*Department of Physics, University of California, Berkeley, California 94720, USA*
[5]*Nuclear Science Division, Lawrence Berkeley National Laboratory, Berkeley, California 94720, USA*
[6]*Department of Physics, William & Mary, Williamsburg, Virginia 23187, USA*

(Received 5 September 2023; accepted 2 April 2024; published 26 April 2024)

The Efimov phenomenon manifests itself as an emergent discrete scaling symmetry in the quantum three-body problem. In the unitarity limit, it leads to an infinite tower of three-body bound states with energies forming a geometric sequence. In this work, we study the evolution of these so-called Efimov states using relativistic scattering theory. We identify them as poles of the three-particle S matrix in the complex energy plane, and we study how they transform from virtual states through bound states to resonances when we change the interaction strength. We dial the scattering parameters toward the unitarity limit and observe the emergence of the universal scaling of energies and couplings—a behavior known from the nonrelativistic case. We additionally find that Efimov resonances follow unusual, cyclic trajectories accumulating at the three-body threshold and then disappear at some values of the two-body scattering length. We propose a partial resolution to this "missing states" problem.

DOI: 10.1103/PhysRevA.109.043325

I. INTRODUCTION

The discovery of the Efimov effect in 1970 revealed the formation of an infinite number of bound states, or trimers, in a system of three nonrelativistic bosons [1,2]. Assuming they interact via two-body forces characterized by a large scattering length, the three-body binding energies form a geometric sequence with a quotient $\lambda^2 \approx 515$. The emergence of the phenomenon is closely tied to the scale invariance of the quantum-mechanical $1/r^2$ potential [3–6], and it is the best known example of the renormalization-group limit cycle [7–10].

The sequence of trimers becomes infinite in the so-called unitarity limit, i.e., when the two-body scattering length, a, is made arbitrarily large, $a \to \infty$. While such behavior has not been observed in nature, several nuclear [11–14] and hadronic systems [15–19] may serve as proxies due to their large scattering length. Furthermore, Efimov physics is realized experimentally using ultracold atoms submerged in a background magnetic field tuned to introduce a Feshbach resonance and drive the system to the unitarity limit [20–32]. Given the generality of the result, this phenomenon has ignited a rich line of research into universality across different subfields [33–47].

Although the unitarity limit does not seem to exist in nature, we can expose the universal scaling behavior by exploring the evolution of Efimov states in the vicinity of this limit. We investigate this evolution using relativistic scattering theory, which has been derived as part of ongoing efforts to develop a model-independent framework for studying three-body systems [48–60]. Building on previous work [61], we identify the trimers as poles of the S matrix in the complex energy variable, and we study their behavior for various values of a, including the $a \to \infty$ limit. We provide evidence of the discrete scaling relationship between the binding energies of the three-body spectrum,

$$\Delta E_n(a) = Q_a^2\, \Delta E_{n+1}(Q_a a), \tag{1}$$

where ΔE_n is the binding energy of the nth bound state, and Q_a is a scaling quotient that asymptotes to Efimov's λ in the unitarity limit. This scaling relationship holds as the states evolve from bound states to unstable resonances, verifying that the relativistic framework recovers the known nonrelativistic results.

Similar three-body models were previously studied using Faddeev equations [62–67] and nonrelativistic effective field theories [9,68,69]. In particular, the authors of Refs. [70–72] made noteworthy progress in the analysis of Efimov resonances. First attempts to understand the system of three bosons in the relativistic framework have been made in Refs. [73,74]. However, their result disagreed with the subsequent light-front calculation [75] obtained in an equivalent regularization scheme. Its redefinition [76] led to an approximate agreement between two approaches but also implied the unphysical behavior of the trimer mass becoming imaginary

*dawids@uw.edu
†m2islam@odu.edu
‡rbriceno@berkeley.edu
§awjackura@wm.edu

at finite values of a. We do not observe any indication of the Thomas collapse reported in this work.[1]

Nevertheless, by studying the analytic structure of the scattering amplitude, we find a much richer picture of the trimers' behavior than previously identified. We discuss intriguing properties of their evolution across various unphysical Riemann sheets of the complex energy plane, such as the formation of cyclic trajectories of the three-body poles and the emergent scaling property of the associated residues. Moreover, we identify a new, "quirky" state following a fractal trajectory in the upper half of the unphysical Riemann sheet. The behavior of the Efimov resonances is sufficiently puzzling that it motivates us to conjecture about the structure of the three-boson amplitudes and to call for further investigation of these states.

We organize this article in the following manner. Section II reviews the relativistic three-body framework used to study the universality of three bosons. It also contains a brief description of the analytic continuation of the three-body scattering amplitude to the regions of the complex energy plane where Efimov states appear. Section III presents the main numerical results of this work, showing evidence for Efimov trimers, and it discusses their behavior as the poles of the $3 \to 3$ amplitude. Finally, the article concludes with a summary in Sec. IV. The article has three technical Appendixes.

II. THREE-BODY SCATTERING

We consider scattering of three identical spinless bosons of mass m, labeled as "φ," in their center-of-mass (c.m.) frame. We assume the system's total angular momentum is $J = 0$, and we neglect contributions from the two-particle subsystems of angular momentum higher than zero. The partial-wave projected $3\varphi \to 3\varphi$ amplitude, $\mathcal{M}_3$, depends on the total relativistic energy E and two more variables. We describe the system by splitting the scattering states into a *spectator* particle and a *pair*, formed from the two other bosons, and we use magnitudes of initial and final spectator momenta, $k = |\boldsymbol{k}|$ and $p = |\boldsymbol{p}|$, as the remaining kinematic parameters. In what follows, we use a notation where all amplitude-like objects have an implicit energy dependence, e.g., $\mathcal{M}_3(p, k; E) \equiv \mathcal{M}_3(p, k)$.[2]

A. The integral equations

To describe the scattering process, we employ the relativistic on-shell three-body equations defined in Ref. [49]. The amplitude is expressed as a sum of two objects,

$$\mathcal{M}_3(p, k) = \mathcal{D}(p, k) + \mathcal{M}_{\mathrm{df},3}(p, k). \tag{2}$$

The first term is called the *ladder* amplitude, and it describes the scattering driven by one-particle exchanges, with the three-body couplings "turned off." The second term describes a probability of an interaction due to short-range forces and potential rescattering effects in the final and initial state.

The equation for the S-wave projection [61,81,82] of $\mathcal{D}$ is

$$\mathcal{D}(p, k) = -\mathcal{M}_2(p)\, G(p, k)\, \mathcal{M}_2(k) - \mathcal{M}_2(p) \int_{k'} G(p, k')\, \mathcal{D}(k', k). \tag{3}$$

The integral is defined as $\int_k \equiv \int_0^{k_{\max}} \mathrm{d}k\, k^2/(2\pi)^2 \omega_k$, where $k_{\max}$ is the maximum allowed value of the momentum, and $\omega_k = \sqrt{m^2 + k^2}$ is the intermediate spectator energy. The amplitude $\mathcal{D}$ depends on two dynamic inputs: the $2\varphi \to 2\varphi$ scattering amplitude, $\mathcal{M}_2$, governed by the two-body interactions within a pair, and the single-particle propagator, G, describing the probability of a particle exchange (flip) between external pairs.

For sufficiently low energies of the interacting pair, the S-wave amplitude $\mathcal{M}_2$ is described well in the leading-order effective range expansion,

$$\mathcal{M}_2(k) = \frac{16\pi\, \varepsilon_k}{-1/a - i q_k}, \tag{4}$$

where $\varepsilon_k = \sqrt{(E - \omega_k)^2 - k^2}$ is the pair's energy in its c.m. frame, and $q_k = \sqrt{\varepsilon_k^2/4 - m^2}$ is the relative momentum between the particles in the pair. Parameter a is the two-body scattering length. Here, we employ this model regardless of the energy ε_k.

Due to the square root in the definition of the relative momentum, one defines the two-body amplitude on two Riemann branches in the complex ε_k variable. The first is the physical sheet given by condition $\mathrm{Im} q_k > 0$, and the second (unphysical) sheet is described by $\mathrm{Im} q_k < 0$. Regardless of the value of $|ma| \geqslant 1$, the $\mathcal{M}_2$ amplitude has a pole in the ε_k variable, corresponding to a state with mass $m_b = 2\sqrt{m^2 - 1/a^2}$. It resides on the real axis below the two-body threshold, $\varepsilon_k < 2m$. If $a > 0$, the pole is on the first sheet and is associated with a two-body bound state. Otherwise, it is a virtual state on the second sheet.

The form of the on-shell one-particle exchange (OPE) amplitude G is partially fixed by the three-body S matrix unitarity. It is given by the relativistic boson propagator,

$$G(\boldsymbol{p}, \boldsymbol{k}) = \frac{1}{(E - \omega_p - \omega_k)^2 - (\boldsymbol{p} + \boldsymbol{k})^2 - m^2 + i\epsilon}. \tag{5}$$

Projecting it to the total S wave produces a kinematic function $G(p, k)$ with logarithmic branch cuts,

$$G(p, k) = -\frac{1}{4pk} \log\left(\frac{z(p, k) + i\epsilon - 2pk}{z(p, k) + i\epsilon + 2pk}\right). \tag{6}$$

Here $z(p, k) = (E - \omega_k - \omega_p)^2 - k^2 - p^2 - m^2$. The OPE amplitude describes a long-range interaction between the pairs, which, in addition to large scattering length a, is

[1] One can find additional studies in Refs. [77–80] and a review of the situation in Ref. [42].

[2] Strictly speaking, in this article we work with the pair-spectator amplitude $\mathcal{M}_3^{(u,u)}$, where specific spectators are chosen. The superscript emphasizes that the initial and final states are "unsymmetrized." It becomes the genuine $3\varphi \to 3\varphi$ amplitude $\mathcal{M}_3$ only after symmetrization with respect to different spectator choices [49]. Keeping that in mind, we drop the (u, u) superscript from all the amplitude-like objects.

necessary to generate the Efimov spectrum.[3] The second term of Eq. (2), amplitude $\mathcal{M}_{\mathrm{df},3}$, depends on $\mathcal{D}$ and the so-called three-body K matrix, $\mathcal{K}_3$, which describes short-distance dynamics of three particles.[4] In this article, we consider the simplest scenario (the so-called isotropic approximation) where it depends solely on the total energy of the system, $\mathcal{K}_3(p,k) \equiv \mathcal{K}_3(E)$. In practice, it is an unconstrained function of E consisting of a polynomial of arbitrary order and a sum of poles. We note that $\mathcal{K}_3$ is a regularization-scheme-dependent object; thus, any choice of $\mathcal{K}_3$ fixes the cutoff momentum. Changes in the regularization lead to a different three-body K matrix, assuring that the full three-body amplitude, $\mathcal{M}_3$, is independent of the cutoff.

The amplitude $\mathcal{M}_{\mathrm{df},3}$ takes a form

$$\mathcal{M}_{\mathrm{df},3}(p,k) = \mathcal{L}(p)\,\frac{1}{\mathcal{K}_3^{-1} + F_3^{\infty}}\,\mathcal{L}(k), \tag{7}$$

where the "end cap" functions describing two-body rescattering contributions are

$$\mathcal{L}(p) = \frac{1}{3} - \mathcal{M}_2(p)\rho(p) - \int_{k'} \mathcal{D}(p,k')\rho(k'). \tag{8}$$

The three-body kinematic function, F_3^{∞}, describes the effects of propagation of on-shell three-body states interacting either within two-body subchannels or via one-particle exchanges. It is expressed in terms of $\mathcal{M}_2$ and the $\mathcal{D}$ amplitude,

$$F_3^{\infty} = \int_{k'} \rho(k')\,\mathcal{L}(k'). \tag{9}$$

Finally, the phase space function, ρ, is defined as[5]

$$\rho(k) = -\frac{iq_k}{16\pi\,\varepsilon_k}. \tag{10}$$

Following our previous work in Refs. [61,81], we numerically solve the above integral equations to obtain $\mathcal{M}_3$ in the complex energy plane on the physical and the nearest unphysical sheets.

B. Trimer poles and thresholds

Scattering states are associated with poles of the amplitude, with a residue corresponding to the coupling of the state to an open channel. Lehmann-Symanzik-Zimmerman [83–86] reduction implies that this identification holds for poles on and off the real energy axis. Causality assures that a complex-valued singularity cannot reside on the "physical" energy plane and must instead appear in unphysical Riemann sheets generated by square-root and logarithmic branch cuts of the scattering amplitude. Depending on the location in the complex plane and the sheet, these poles are associated with bound states (real-valued, physical sheet), virtual states (real-valued, unphysical sheet), or resonances (complex-valued, unphysical sheet).

The relativistic three-body amplitude, $\mathcal{M}_3(p,k)$, exhibits poles associated with trimers in the E^2 plane. Near the nth pole, it behaves like

$$\mathcal{M}_3(p,k) = -\frac{\Gamma_n(p)\,\Gamma_n(k)}{E^2 - E_n^2} + \cdots, \tag{11}$$

where E_n is the trimer energy, and ellipses indicate higher-order terms. Bound or virtual states have $\mathrm{Im}E_n = 0$, while resonances have $\mathrm{Im}E_n \neq 0$. The residue, i.e., the coupling of the nth trimer to the 3φ state, factorizes into momentum-dependent vertex factors $\Gamma_n(k)$ that are closely related to the Faddeev wave functions in the nonrelativistic limit.

To access the trimer poles of $\mathcal{M}_3$, one needs to extend the solution of the integral equation from physical to complex values of kinematic variables p, k, and E. Analytic continuation to the complex plane depends on the nature of the singularities of the three-body scattering amplitude encoded in Eq. (3). In addition to potential poles, the $\mathcal{M}_3$ amplitude has a logarithmic branch cut inherited from the partial-wave projected propagator, G. Furthermore, it has two possible physical thresholds manifesting as corresponding branch points. These are the square-root bound-state-spectator threshold at $E_{\mathrm{thr}}^{(\varphi b)} = m + m_b$ and the logarithmic three-body threshold at $E_{\mathrm{thr}}^{(3\varphi)} = 3m$ [87,88]. Unphysical sheets are associated with these two singularities.

The emergence of these thresholds in Eq. (2) has a nonperturbative origin. The three-body amplitude inherits the singularities of $\mathcal{M}_2$ in the external momentum variables, p and k. The threshold branch points of $\mathcal{M}_3(p,k)$ in the E^2 plane emerge from the second term of Eq. (3) when these energy-dependent singularities in the k' variable coincide with the origin of the integration interval, $k' = 0$ [61,88,89]. The branch cut at $E = E_{\mathrm{thr}}^{(\varphi b)}$ arises from the collision of point $k' = 0$ with the two-body bound-state pole. The $E_{\mathrm{thr}}^{(3\varphi)}$ branch point appears from the collision with the square-root branch point of $\mathcal{M}_2$.

To extend $\mathcal{M}_3$ to the unphysical Riemann sheets of the E^2 plane, either through the φb or the 3φ cut, one needs to avoid integrating over the discontinuities associated with the above-mentioned collisions, i.e., avoid coincidence of the integration interval with the pole or threshold cut in k'. We accomplish this by deforming the integration contour into the complex k' momentum plane. In doing this, we ensure that the deformed integration path avoids logarithmic branch points of $G(p,k')$ and all other singularities induced by the nonperturbative nature of the equation [6]. The reader can find a detailed description of this procedure in Appendix A.

III. EFIMOV TRIMERS

In the remainder of this work, we set $\mathcal{K}_3 = 0$. This choice is motivated by the desired simplicity of the discussion and

[3]References [61,81] employ smooth regularization of the integral equation, implemented by multiplying $G(p,k)$ by an exponentially falling function $H(p,k)$. Here, we use the hard cutoff version of $H(p,k)$ that is equal to 1 in the range of integration and 0 otherwise. It implies $k_{\max} = (E^2 - m^2)/2E$ for the maximal value the momentum can take. It corresponds to minimal $\varepsilon_{k'} = 0$ of the pair in the intermediate three-body state.

[4]Compared to Refs. [48,49], we drop the "df" label from this object to simplify the notation.

[5]It differs slightly from Refs. [48,49], where the phase space was proportional to the cutoff function. We also drop the "3" subscript from the definition of the phase space to simplify the notation.

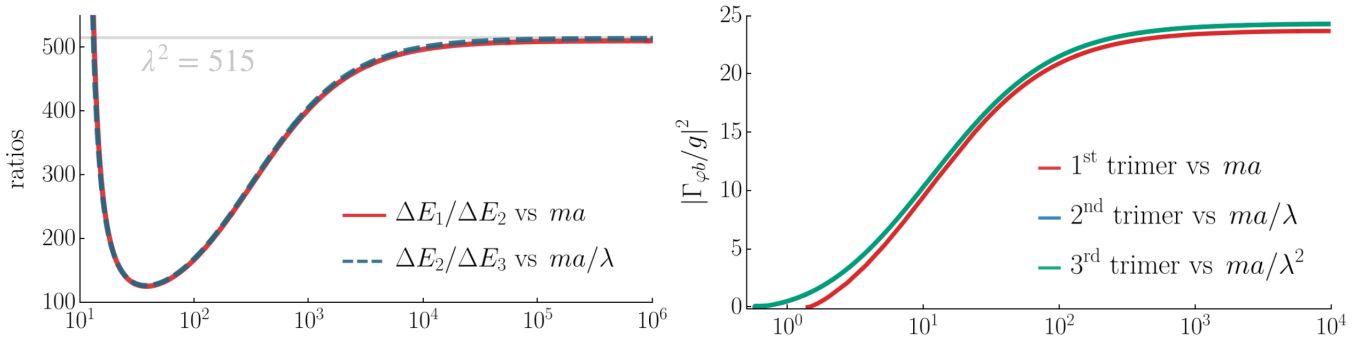

FIG. 1. Left panel: ratios of subsequent binding energies vs ma (x-axis). The horizontal axis for $\Delta E_1/\Delta E_2$ (dashed line) is rescaled by λ. We show the Efimov ratio, λ^2, as a horizontal, gray line. Right panel: normalized residues of the first three bound-state poles of the $\mathcal{M}_{\varphi b}$ amplitude as functions of ma. The bottom red graph corresponds to the ground state. The upper two curves correspond to excited states (indistinguishable within the numerical precision). The scattering lengths for these residues are rescaled by appropriate powers of λ, as indicated in the legend.

does not affect the generality of the presented results. For interested readers, we discuss the nonzero case in Appendix B, where we argue that the universal scaling behavior of poles is independent of $\mathcal{K}_3$.

A. Bound-state poles and residues

Close to the unitarity limit, i.e., for $|ma| \gg 1$, we find that $\mathcal{M}_3$ develops multiple bound-state poles. We observe that their binding energies, $\Delta E_n = E_n - E_{\text{thr}}^{(3\varphi)}$, obey the discrete scaling symmetry given in Eq. (1), which is characteristic of the Efimov phenomenon. The quotient $Q_a \to \lambda$ as $ma \to \infty$, confirming that the relativistic framework recovers the expected Efimov scaling when the binding energies become small compared to the scale-invariance breaking quantities like m or the cutoff k_{max}. At small values of $a > 0$, the ground state exhibits a noticeable deviation from the scaling behavior. Nevertheless, its qualitative features (e.g., pole trajectory, residues) remain analogous to shallow trimers of nonrelativistic binding energies. In agreement with Efimov's prediction, the discrete scaling symmetry emerges not only in the unitarity limit but for finite values of a as well (with $Q_a \neq \lambda$).

This is shown on the left panel of Fig. 1, where the ratios of subsequent binding energies approach the square of Efimov's constant in the unitary limit. Extrapolated values are 0.7% away from λ^2 for the $\Delta E_1/\Delta E_2$ ratio, and 0.001% for the $\Delta E_2/\Delta E_3$ one, which we consider an excellent agreement. For finite values of ma, both ratios show a similar functional dependence on the scattering length. Although the energies exhibit a dependence on $\mathcal{K}_3$, their ratios are mostly independent of its value, in agreement with the argument made in Appendix B.

On the right panel of Fig. 1, we show that the analogous property holds for the residues associated with the trimer poles. At positive values of a, we reduce the three-particle to the bound-state-particle amplitude, $\mathcal{M}_{\varphi b}$ [introduced in Eq. (A1)], and we extract the residues from the Laurent expansion,

$$\mathcal{M}_{\varphi b} = -\frac{|\Gamma_{\varphi b}|^2}{E^2 - E_n^2} + \cdots . \tag{12}$$

Residue $|\Gamma_{\varphi b}|^2$ describes the coupling strength between the trimer and the φb state. We normalize it with the two-body coupling g^2 and plot it as a function of ma. As we can see, rescaling the characteristic length scales brings all residues close to each other, with almost no difference between the second and the third trimer and an $O(10\%)$ discrepancy between these two and the first one. Despite the relatively small binding energy of the deep bound state, we understand it as a remnant of relativistic effects in the formation of this state.

Finally, in Fig. 2, we verify numerically the known analytic form for the nonrelativistic vertex function, which was derived in Ref. [90] and confirmed in Ref. [91],

$$|\Gamma(k)|^2 = |c||A|^2 \frac{256\pi^{5/2}}{3^{1/4}} \frac{m^2\kappa^2}{k^2(\kappa^2 + 3k^2/4)} \times \frac{\sin^2(s_0 \sinh^{-1}(\sqrt{3}k/2\kappa))}{\sinh^2(\pi s_0/2)}. \tag{13}$$

Here, $\kappa = -\sqrt{|m\Delta E|}$ and $s_0 \approx 1.006$. Normalization constant $|c| = 96.351$, while A is close to 1 when $ma \to \infty$. The plot in Fig. 2 was obtained for the first three trimers at $ma = -10^6$, which corresponds to binding

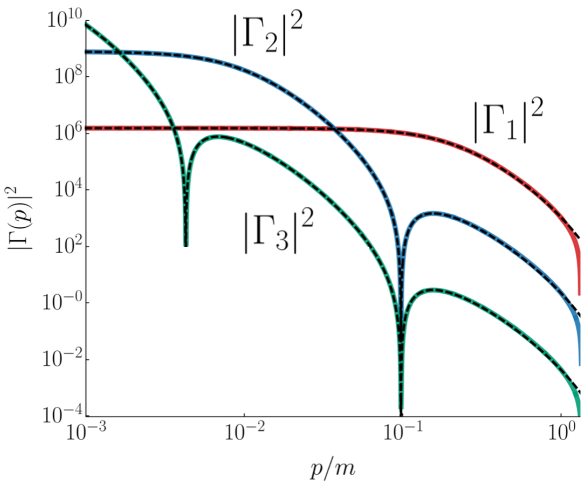

FIG. 2. Residues of the $\mathcal{M}_3$ amplitude at the first three trimer poles for $ma = -10^6$. Dashed black lines represent the analytic prediction of Ref. [90].

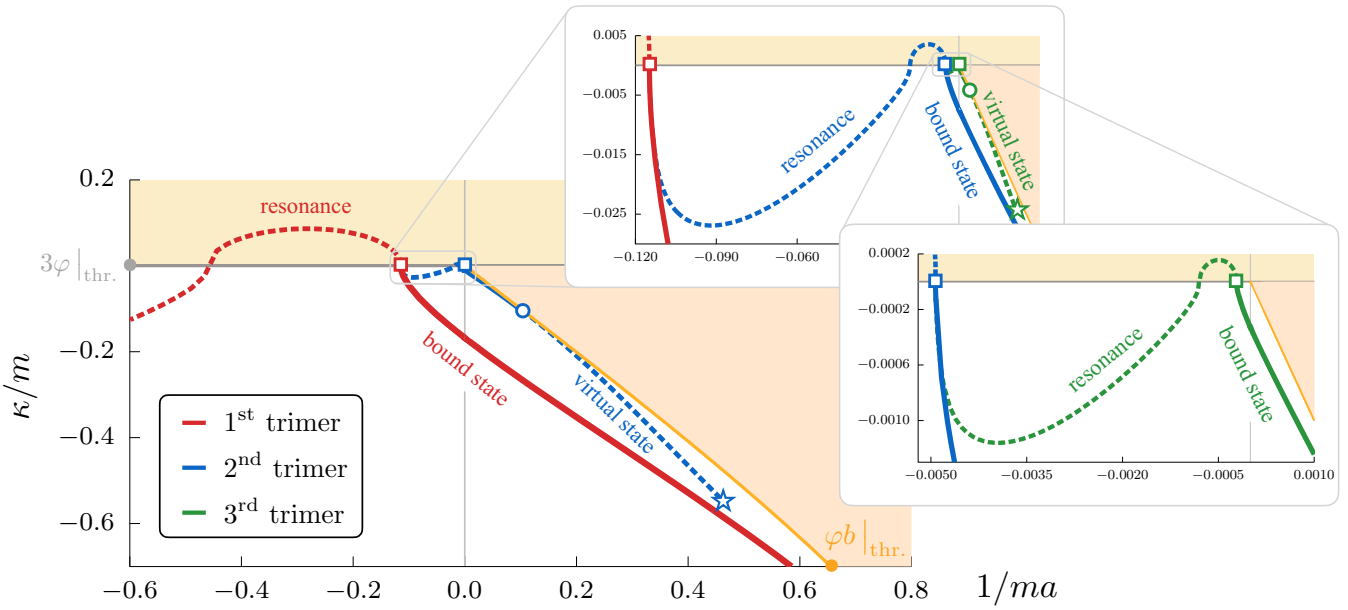

FIG. 3. Trajectories of the first three trimer poles in the $(\kappa/m, 1/ma)$ plane where $\kappa = \text{sgn}(\text{Re}\Delta E)\sqrt{|m\text{Re}\Delta E|}$ (states are ordered by their distance from the φb threshold). The 3φ and φb thresholds are shown explicitly as gray and orange lines. Solid lines denote physical bound states, while dashed ones denote either virtual bound states on the unphysical φb sheet or resonances on the nearest 3φ sheet. Stars denote the emergence of a virtual state from the logarithmic cut on the second φb sheet. Circles denote the evolution of this virtual state onto a real bound state. Squares denote the further evolution of the state to three-body resonance. Insets show the behavior of trimers near the three-body threshold.

energies: $\Delta E_1/m = -2.8 \times 10^{-2}$, $\Delta E_2/m = -5.5 \times 10^{-5}$, and $\Delta E_3/m = -1.1 \times 10^{-7}$. The presented agreement of the nonrelativistic result with our finding is another confirmation that the observed states are undoubtedly Efimov in nature. As expected, we can observe a discrepancy between our numerical result and the analytic formula for momenta that can be considered relativistic, $p/m = O(1)$.

B. Virtual states and resonances

By dialing ma to smaller values, we trace the trimers on their trajectories that span across multiple Riemann sheets associated with the dimer-particle and three-particle cuts. The trimers evolve from the virtual states (small, positive a) through bound states (large a of both signs) to resonances (small, negative a). In Fig. 3, we present their trajectories on the so-called Efimov plot, i.e., in the $(\kappa, 1/a)$ plane, where the (generalized) binding momentum $\kappa = \text{sgn}(\text{Re}\Delta E)\sqrt{|m\text{Re}\Delta E|}$.

All excited states follow similar trajectories. They emerge as virtual states on the unphysical φb sheet from the logarithmic cut inherited by $\mathcal{M}_3$ from the one-particle exchange amplitude, G. They approach the dimer-particle threshold and move to the first sheet, becoming bound states. They remain bound states for large negative values of a and evolve to become resonances on the nearest unphysical sheet associated with the logarithmic 3φ threshold cut.

We trace their motion on this sheet, in the complex ΔE variable, and present it in Fig. 4. (See also the Supplemental Material for a video of the info presented in Fig. 4 [92].) At a given finite value of ma, there is only a single resonance pole in the unphysical sheet. As we decrease ma from zero to $ma = -8.71$, the "ground-state" resonance moves to the three-body threshold on an arc from complex infinity. It is natural since $ma \to 0$ corresponds to no dynamics and the removal of all but the free states from the spectrum.

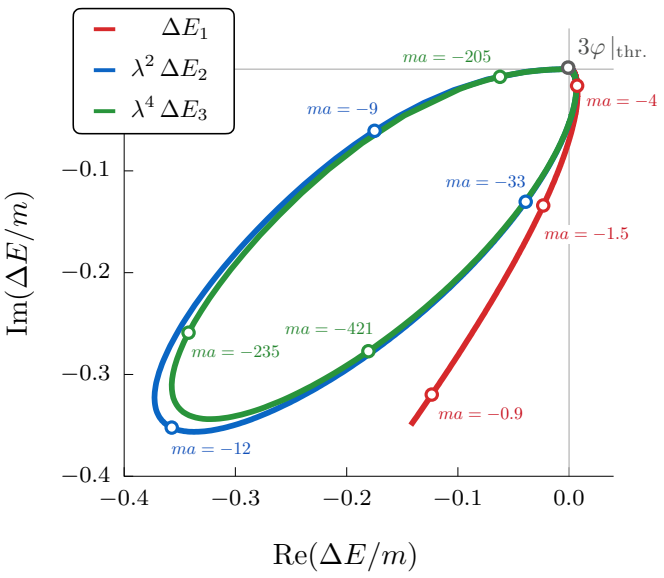

FIG. 4. Trajectories of the first three resonances on the nearest unphysical Riemann sheet of the complex ΔE plane. Energies of the second and third trimers are rescaled by λ^2 and λ^4, respectively. At large $|ma|$ and close to the threshold, all trajectories exhibit discrete scaling symmetry. As $|ma|$ decreases, the scaling symmetry breaks down, although for the second and third resonant states the discrepancy between the trajectories remains small.

By contrast, the excited three-body resonances follow cyclic trajectories, which start and end at the three-body threshold and accumulate near this point. By rescaling them by an appropriate power of λ^2, we observe that they nearly overlap, providing additional evidence of the discrete scale invariance in the three-boson system. Similar trajectories of the Efimov resonances were previously noticed in Refs. [66,93], where a nonrelativistic approach was used.

Moreover, we discover an interesting pattern as these excited trimers move between the physical and unphysical Riemann sheets. Namely, the first excited resonance of energy ΔE_2 emerges from the threshold on the unphysical sheet at the same value, $ma = -8.71$, at which the ground-state resonance reaches this point and becomes a bound state on the physical energy plane. It leads to a "missing poles" problem: one pole reaches the threshold, and two emerge. This behavior is repeated for all states, i.e., whenever the nth resonance enters the threshold, the $(n+1)$th resonance appears on the unphysical sheet, and the nth bound state appears on the physical one. Furthermore, we find that the residues of all three poles converge to the same value when they approach the 3φ branch point; see Appendix C

This puzzling behavior violates our expectation that the number of poles, equivalent to the number of physical states, must be conserved when one varies the theory parameters [94]. The only exception is the instance of lifted spectrum degeneracy, which we verify does not happen in our system by studying the order of trimer poles.

We propose a possible resolution to this puzzle by noting that the three-body scattering amplitude has infinitely many unphysical sheets; see Fig. 5. We label the two nearest sheets ± 1 while denoting the physical sheet by 0. States in the -1 plane are the complex-conjugate or "*mirror*" poles of those in the $+1$ sheet. This is unlike the two-body case, where the Schwarz reflection principle ensures that a resonance pole has its mirror image on the same sheet. For the three-body amplitude, similarly to a complex logarithm, it implies a reflection between the $\pm n$ sheets.

We conjecture that the missing poles come from the higher Riemann branches, one from each. The nth state approaches the threshold from complex infinity on the nth Riemann sheet and moves to the $(n-1)$th one, where it starts evolving on a cyclic trajectory. Eventually, in the unitarity limit, it travels to the physical energy plane, contributing to the geometric sequence of bound states. We depict this idea in Fig. 5, where the dashed lines represent trajectories of $n \geqslant 4$ states. References [66,93] did not address the "missing poles" issue.

One could verify this conjecture by analytically continuing the amplitude to the higher Riemann sheets. Although we were unable to extend our solution to the other sheets, we have performed numerical extrapolations presented in Appendix C that further support this conjecture. Our proposal only partially resolves the puzzle. Whenever a resonance approaches the threshold, its "mirror" image does the same. Yet, we observe only one bound state emerging on the physical energy plane. The "mirror" poles seem to vanish when meeting their complex-conjugate partners at the threshold, which, again, violates our expectation about the conservation of the number of states.

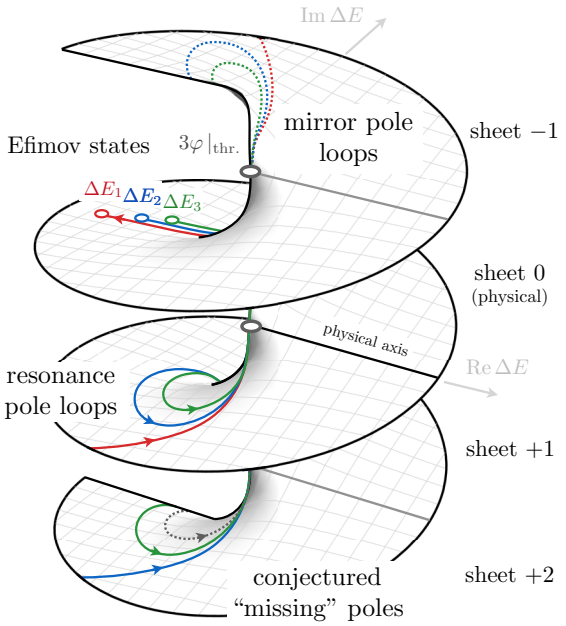

FIG. 5. Riemann surfaces of the three-body amplitude in ΔE. The trajectories of the trimers are shown, along with three bound-state positions for some a. On the nearest unphysical sheet, the second and third trimers exhibit the cyclic behavior as shown in Fig. 4. Mirror poles are found by continuing up to sheet -1. We postulate that the higher trimers come from the further unphysical sheets ($\geqslant +2$), where their cyclic behavior repeats.

C. Additional "quirky" pole

In addition to the regular Efimov resonances in the $+1$ Riemann sheet of the complex E^2 plane, we also find a new, "quirky" state in the upper half-plane, $\text{Im}E^2 > 0$. We trace its trajectory with the changing two-body scattering length and we present it in Fig. 6, denoting its binding energy as ΔE_q. We observe as it approaches the three-body threshold from a deep region of the complex plane, supposedly the complex infinity. Interestingly, as the magnitude of ma increases, it bypasses the three-body branch point and turns back. This pattern keeps repeating for arbitrarily high values of ma. The fractal trajectory it forms has a self-similarity factor converging to Efimov's constant, λ^2, as we dial $a \to \infty$.

We find this state unexpected, and, at this point, we cannot draw any conclusions on its nature. The pole approaches the three-body branch point in the unitarity limit and could play a role in the accumulation of bound-state poles at the threshold. It could be a physically interesting phenomenon or simply an artifact of the relativistic integral equations. At this time, neither option can be ruled out, and further investigation is needed.

IV. CONCLUSION

To summarize, we found and presented the emergence of the Efimov effect from the relativistic three-body scattering equations. In particular, we discovered evidence of the discrete scaling symmetry in the trajectories of resonances in the nearby unphysical sheet of complex energy. By studying the evolution of the spectrum onto unphysical sheets, we make

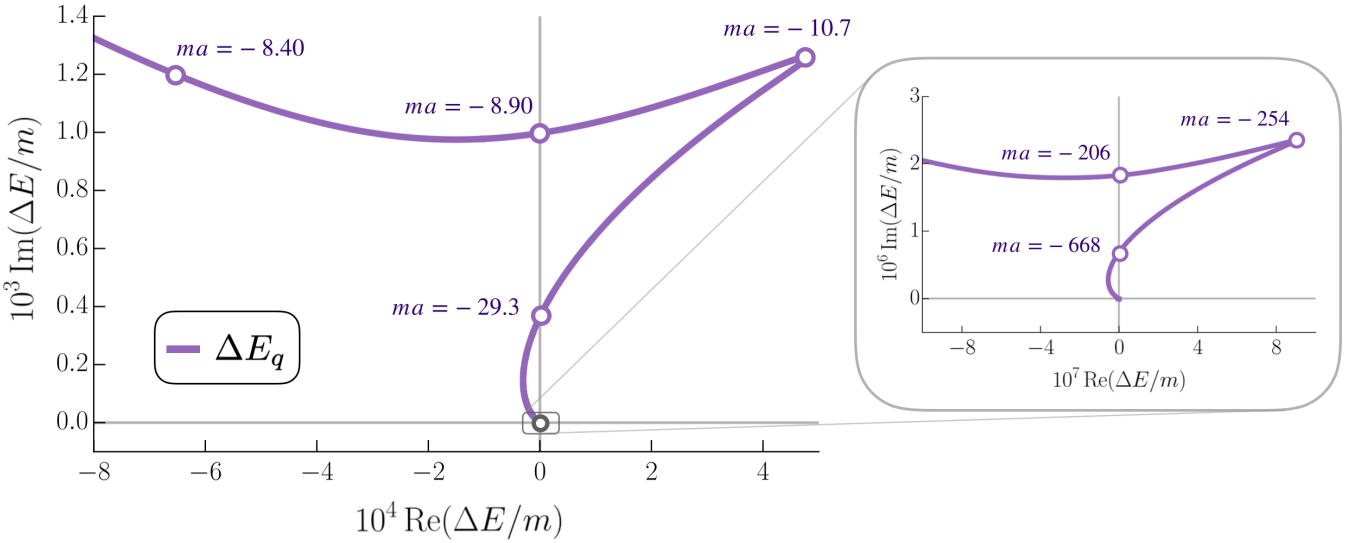

FIG. 6. Evolution of the "quirky" pole in the upper half-plane of the +1 Riemann sheet. The pole approaches the threshold from complex infinity. As $|ma|$ decreases, its trajectory forms a fractal pattern with rescaling quotient converging to λ^2.

several observations suggesting that the Efimov phenomenon is closely related to the logarithmic nature of the three-body unitarity cut, i.e., the presence of infinitely many branches. At the same time, our conjecture about the behavior of the trimer trajectories cannot be the end of the story because of the mirror fashion in which + and − sheets contribute trimer poles to the physical sheet.

The "missing pole" problem is not just a mathematical curiosity but points to a deficiency in our knowledge about the analytic structure and properties of three-particle scattering amplitudes. This, in turn, affects our understanding of the nature of particles that couple strongly to three-particle states [95–104]. Having relativistic scattering amplitudes that satisfy unitarity and whose analytic structure we can fully control will impact a broad set of experimental, phenomenological, and lattice QCD studies. As a result, we close by encouraging further investigations along these lines.

ACKNOWLEDGMENTS

The authors thank T. Hyodo, S. Sharpe, M. Baker, and S. Mizera for valuable discussions. S.M.D. is supported by U.S. Department of Energy Contract No. DE-SC0011637. R.A.B. and M.H.I. acknowledge the support of the U.S. DOE Early Career award, Contract No. DE-SC0019229. M.H.I. acknowledges the support from the Jefferson Science Associates/Jefferson Lab graduate fellowship program. A.W.J. acknowledges the support of the U.S. DOE ExoHad Topical Collaboration, Contract No. DE-SC0023598.

APPENDIX A: ANALYTIC CONTINUATION

Here, we briefly describe the analytic continuation of the integral equation defining the $\mathcal{D}(p,k)$ amplitude. We wish to extend it from the real axis to the complex energy, which is achieved by the method of the integration contour deformation. Generalization of the integration interval from a straight real line to a complex curved path is motivated by the presence of movable (energy-dependent) singularities of $G(p,k')$, $\mathcal{M}_2(k')$, and $\mathcal{D}(k',k)$ that can cross the real k' momentum axis when E^2 becomes complex-valued. These singularities must be avoided at each value of E^2 and p; otherwise, the final result becomes contour-dependent, invalidating the uniqueness of the analytic continuation.

The main focus of this article, i.e., identification of the trimer states as poles of the amplitude, requires a solution of the integral equation for real energies below the φb and 3φ thresholds and for complex energy in the unphysical Riemann sheets associated with these two branch cuts. We first briefly summarize methods employed in Refs. [61,81] to analyze the φb system, and only then we describe the continuation of the amplitude through the three-body cut. We focus on the $\mathcal{K}_3 = 0$ case for clarity of presentation. Once we compute the ladder amplitude from Eq. (3), we can obtain the full $\mathcal{M}_3$ amplitude by utilizing the remaining formulas in Sec. II.

1. The dimer-particle threshold

In Ref. [60], we explained how the scattering amplitude between a two-body bound state and a spectator, $\mathcal{M}_{\varphi b}$, is obtained from the three-body scattering amplitude using the LSZ reduction formula. The amplitude $\mathcal{D}(p,k)$ has poles at values of the pairs' energies squared, ε_p^2, ε_k^2, equal to that of the bound state, m_b^2. The residue of the three-body amplitude at these poles is proportional to $\mathcal{M}_{\varphi b}$. Explicitly, expanding $\mathcal{D}(p,k)$ in their vicinity, we find

$$\mathcal{D}(p,k) = \frac{g^2\,\mathcal{M}_{\varphi b}(E)}{\left(\varepsilon_p^2 - m_b^2\right)\left(\varepsilon_k^2 - m_b^2\right)} + \cdots, \tag{A1}$$

where $g^2 = 128\pi m_b/a$. Continuing the external spectator momenta, p and k, to the value corresponding to the two-body bound state pole, q_b,

$$q_b = \frac{\lambda^{1/2}\left(E^2, m_b^2, m^2\right)}{2E}, \tag{A2}$$

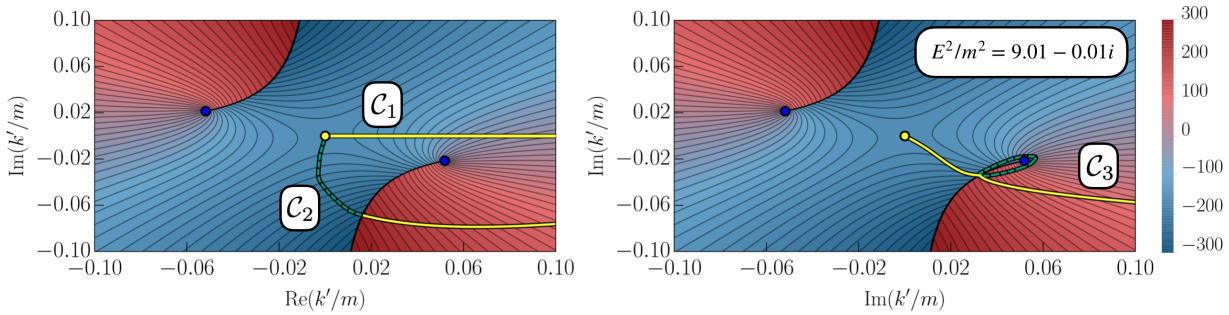

FIG. 7. Imaginary part of $\mathcal{M}_2(k')$ in the complex k' plane for $ma = -6$ and $s/m^2 = 9.01 - 0.01i$. Black lines represent branch cuts, and blue dots are branch points. Three example integration contours are shown. On the left panel, $\mathcal{C}_1$ (yellow, straight line) is the original integration interval of Eq. (3) defining the solution, $\mathcal{M}_3(p,k)$, on the physical Riemann sheet of the complex E^2 plane. To continue the three-body amplitude through the three-body cut, one deforms $\mathcal{C}_1 \to \mathcal{C}_2$. Amplitude $\mathcal{M}_2$ in the integration kernel must be evaluated on its second sheet when k' belongs to the green, dashed piece of $\mathcal{C}_2$. On the right panel, we show an example contour, $\mathcal{C}_3$, defining the ladder amplitude on the $+2$ unphysical Riemann sheet of the E^2 plane.

brings $\varepsilon_p^2, \varepsilon_k^2 \to m_b^2$, allowing us to extract the residue from the above formula. Here $\lambda(x,y,z) = x^2 + y^2 + z^2 - 2xy - 2xz - 2yz$ is the Källén triangle function.

The trimer bound and virtual states are poles of the $\mathcal{M}_{\varphi b}$ amplitude below the φb threshold that lie on the first and second Riemann sheets, respectively. From the two-body S matrix unitarity, the analytic continuation of the amplitude to the unphysical Riemann sheet, $\mathcal{M}^{\mathrm{II}}_{\varphi b}$, is known explicitly,

$$\mathcal{M}^{\mathrm{II}}_{\varphi b}(E) = \frac{\mathcal{M}_{\varphi b}(E)}{1 + 2i\rho_{\varphi b}(E)\mathcal{M}_{\varphi b}(E)}, \tag{A3}$$

where $\rho_{\varphi b}(E)$ is a φb phase-space factor,

$$\rho_{\varphi b}(E) = \frac{q_b}{8\pi E}. \tag{A4}$$

Thus, the knowledge of $\mathcal{M}_{\varphi b}$ on the first Riemann sheet is sufficient to recover both the positions of the three-body bound and virtual states.

The main complication in extending the three-body amplitude below the dimer-particle threshold $E^{(\varphi b)}_{\mathrm{thr}}$ is the logarithmic branch cut of the homogeneous and inhomogeneous terms of the integral equation in the p variable. It originates from the OPE partial-wave projected propagator, Eq. (6), present in both of these terms and thus is an "inherited" singularity of the $\mathcal{D}$ amplitude, appearing in its left-hand argument [61]. At a fixed value of momentum k and total energy, the inhomogeneous term of the equation contributes a fixed cut that has to be avoided by the deformed integration contour. In particular, for external momentum $k = q_b$ and $E < E^{(\varphi b)}_{\mathrm{thr}}$, the cut may take a complicated shape resembling a circle; see Fig. 4 in Ref. [61].

The OPE amplitude in the homogeneous part of the equation is evaluated at complex momenta k' along the contour chosen to avoid this fixed quasicircular shape. Since the right-hand argument of $G(p,k')$ takes infinitely many values, this amplitude contributes a whole set of singularities to the left-argument dependence of the ladder amplitude that we call a *domain of nonanalyticity*. Note that this area of the complex k' plane is defined by the specific integration path chosen. The deformed contour must detour this region of the complex plane, a condition we call self-consistency of the integration contour. Only self-consistent integration paths define proper analytic continuation of the integral equation solution. An example domain of nonanalyticity is found in Fig. 8 of Ref. [61].

We refer the reader interested in more details to this work. Once we verified that all singularities of the integration kernel and of the ladder amplitude $\mathcal{D}(k',k)$ are bypassed, we may attempt to solve the integral equation numerically along the deformed contour, as described in Appendix C therein.

2. Three-particle threshold

Analytic continuation of the ladder amplitude through the three-body (logarithmic) cut to the associated unphysical Riemann sheet requires further explanation that is new to this work.

To simplify the discussion, let us amputate the external two-body amplitudes from the integral equation, obtaining,

$$d(p,k) = -G(p,k) - \int_{k'} G(p,k')\,\mathcal{M}_2(k')\,d(k',k), \tag{A5}$$

where $\mathcal{D}(p,k) = \mathcal{M}_2(p)\,d(p,k)\,\mathcal{M}_2(k)$. In addition to deciding whether the behavior of the singularities of the OPE amplitude demands integration contour deformation, one has to consider the singularities of the two-body amplitude, $\mathcal{M}_2$, in the integration kernel. As described in the main text, the singularities of the amplitude in the E variable emerge from the collision of the integration end point with the singularities of $\mathcal{M}_2$ in the integration kernel. The three-body right-hand cut of the three-body amplitude arises when the right-hand, two-body branch point of $\mathcal{M}_2$ at

$$k' = \frac{\lambda^{1/2}(E^2, m^2, (2m)^2)}{2E} \tag{A6}$$

coincides with the lower limit of integration, $k' = 0$. A particular choice of the integration contour behavior around this branch point determines the Riemann sheet of the obtained integral equation solutions; see Fig. 7.

Namely, when the integration contour circumvents the branch point from the top, and the $\mathcal{M}_2$ is evaluated exclusively on its first Riemann sheet, the integral equation defines the amplitude on the first (physical) Riemann sheet above the three-particle threshold. It is not the only available option.

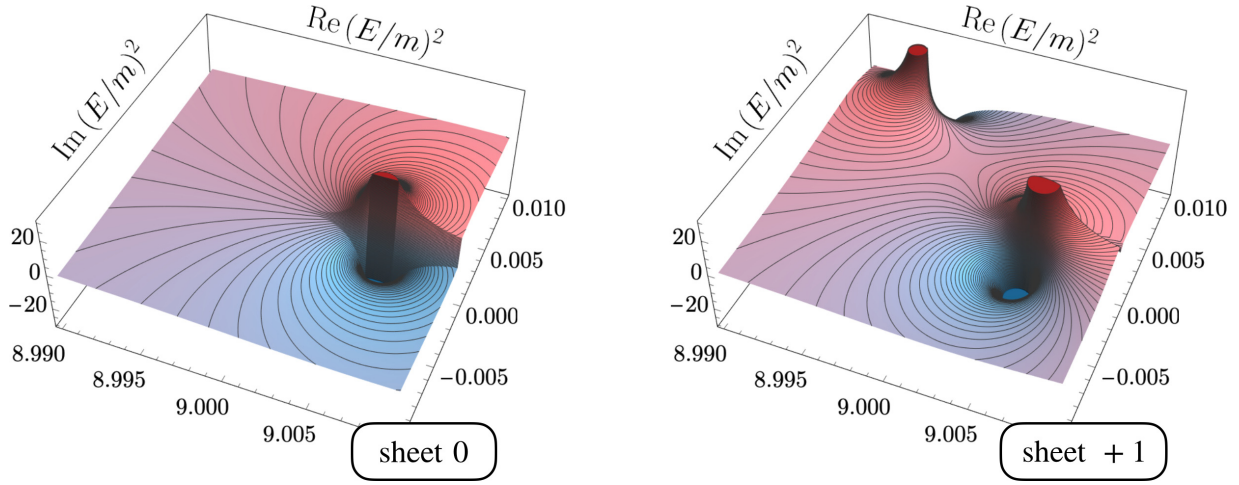

FIG. 8. Imaginary part of the amplitude $m^2\, d(p,k)$ in the complex E^2 plane for $ma = -8.1$ and $\varepsilon_p = \varepsilon_k = 2m^2$. The left panel represents the solution on sheet 0, while the right panel is obtained via the analytic continuation to the nearest unphysical sheet. The "quirky" trimer pole is visible in the right panel, in the upper left corner of the frame.

The integration contour can pass the branch point from the bottom. In this case, the three-body amplitude is computed on its first unphysical $(+1)$ Riemann sheet of the complex E plane. Since there is a cut extending from the $\varepsilon_{k'} = (2m)^2$ point, to properly define the analytic continuation of the three-body amplitude, one must add a relevant discontinuity function to $\mathcal{M}_2$ when evaluating the integration kernel in this case, as indicated by the dashed green line in Fig. 7.

Finally, when the integration contour encircles the branch point n times, as shown in the right panel of Fig. 7, the amplitude is computed on the $(1+n)$th Riemann sheet, using the notation of Fig. 5. We remind the reader that the three-body cut is logarithmic, i.e., contrary to algebraic discontinuities such as in the square root function, it is associated with infinitely many Riemann sheets. Winding around the branch point generates them in the integral-equation representation of the three-body amplitude.

In Fig. 8 we present an example solution of Eq. (A5) for $ma = -8.1$ and external momenta $p = k$ chosen such that $\varepsilon_k^2 = \varepsilon_p^2 = 2m^2$. The solution on the physical Riemann sheet (left panel) exhibits a clear resonance "bump" above the real axis, hinting at a pole on the nearest unphysical sheet. The right panel presents the result of the analytic continuation to the $+1$ branch of the amplitude, which reveals a ground-state pole at position $E_1^2/m^2 \approx 9.0050 - 0.0012i$. It is a pole indicated by the red color in Figs. 3 and 4 in the main text. Another pole, which we called the "quirky" state, is found in the upper half-plane, at position $E/m^2 \approx 8.9944 + 0.0087i$. We also observe another "bump" in the amplitude above the real axis on sheet $+1$, a hint that another pole can be expected on sheet $+2$.

3. Three-particle threshold—sheets $\geqslant +2$

Unfortunately, we found it practically impossible to define integration contours of the type presented in the right panel of Fig. 7 that would be self-consistent, i.e., that would avoid additional singularities generated by the one-particle exchange amplitude. We note that the domain of nonanalyticity always seems to contain the branch point of $\mathcal{M}_2(k')$, meaning that it is unattainable to encircle it with a looplike integration contour without crossing the forbidden area in the complex k' plane. A rigorous solution to the problem of nonconsistency of the integration paths required to extend the three-body amplitude to sheets $\geqslant +2$ needs additional study and is beyond the scope of this paper. As we note in the main text, continuation to the higher Riemann sheets is most probably the solution to the "missing pole" problem and thus will be of practical interest in the future studies of the three-body problem.

APPENDIX B: A NONZERO THREE-BODY K MATRIX

We note that separation into long- and short-range forces is ambiguous since $\mathcal{K}_3$ is a regularization-scheme-dependent object [60]. The cutoff dependence of $\mathcal{D}$ is compensated by the changes of $\mathcal{M}_{\mathrm{df},3}$ under variations of $\mathcal{K}_3$, assuring the scattering amplitude is independent of the regularization choice. In the main text, we consider the case $\mathcal{K}_3 = 0$, for which $\mathcal{M}_{\mathrm{df},3} = 0$ and $\mathcal{M}_3 = \mathcal{D}$. The purpose of this and the subsequent subsection is to argue that this particular choice does not affect our main conclusions. In particular, we would like to verify that near the unitarity, $\mathcal{M}_3$ develops Efimov bound states for a nonzero three-body K matrix.

From Eq. (7), we see that $\mathcal{M}_{\mathrm{df},3}$ contributes poles to the full three-body amplitude whenever

$$\mathcal{K}_3^{-1} + F_3^{\infty}\big|_{E=E_n} = 0. \tag{B1}$$

As a first step, we would like to show that all the poles of $\mathcal{M}_3$ are those described by the above equation. Although it is evident that Eq. (B1) does indeed describe some states, it is not immediately clear that it governs all of them. In particular, the first term in Eq. (2), $\mathcal{D}$, can contribute additional poles to the full three-body amplitude.

Assume $\mathcal{D}$ has a pole at position $E_{n,0}$, i.e., it can be expanded as

$$\mathcal{D}(p,k) = -\frac{\Gamma_{n,0}(p)\Gamma_{n,0}(k)}{E^2 - E_{n,0}^2} + \cdots, \tag{B2}$$

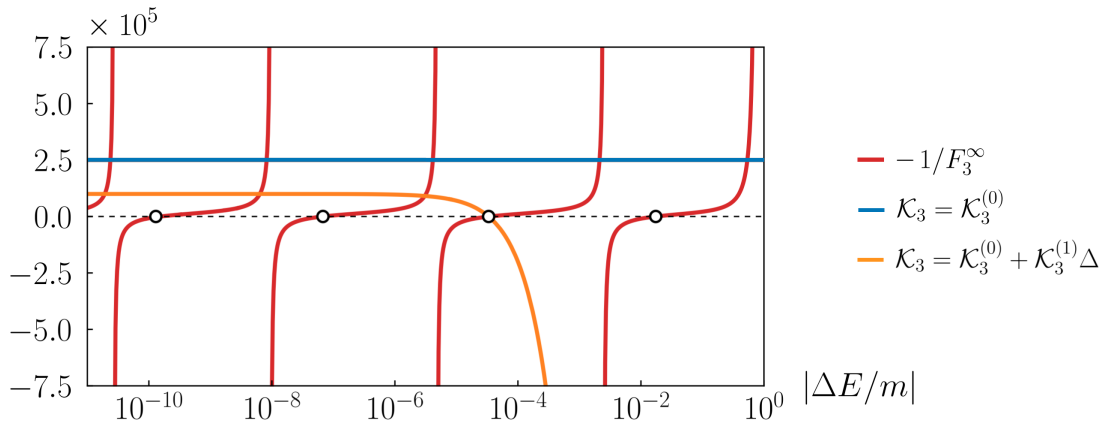

FIG. 9. Inverse $-1/F_3^{\infty}$ as a function of ΔE for $ma = 10^6$ (periodic, red curves). Pole positions of $\mathcal{M}_3$ are determined by crossing with $\mathcal{K}_3$. Two typical forms of $\mathcal{K}_3$ are presented: a constant $\mathcal{K}_3^{(0)}/m = 2.5 \times 10^5$ represented by a horizontal, blue line, and the so-called isotropic approximation represented by a curved orange graph [105,106]. For the latter: $\mathcal{K}_3^{(0)}/m = 10^5$, $\mathcal{K}_3^{(1)}/m = 4.5 \times 10^9$, and $\Delta = (E^2 - (E_{\rm thr}^{(3\varphi)})^2)/(E_{\rm thr}^{(3\varphi)})^2$. Dots represent binding energies in the limit $\mathcal{K}_3 = 0$ for which $\mathcal{M}_3 = \mathcal{D}$.

where the subscript "0" is meant to emphasize that this corresponds to the $\mathcal{K}_3 = 0$ limit of $\mathcal{M}_3$. We note that when $\mathcal{D}$ has a pole in E^2, from Eqs. (8) and (9) it is clear that so do $\mathcal{L}$ and F_3^{∞}. In its vicinity, these functions take the form

$$\mathcal{L}(p) = \frac{\Gamma_{n,0}(p)}{E^2 - E_{n,0}^2} \int_{k'} \Gamma_{n,0}(k')\rho(k') + \cdots, \tag{B3}$$

$$F_3^{\infty} = \frac{1}{E^2 - E_{n,0}^2} \left[\int_{k'} \Gamma_{n,0}(k')\rho(k') \right]^2 + \cdots. \tag{B4}$$

Using these expansions in Eq. (7), we find

$$\mathcal{M}_{\mathrm{df},3}(p,k) = \frac{\Gamma_{n,0}(p)\Gamma_{n,0}(k)}{E^2 - E_{n,0}^2} + \cdots, \tag{B5}$$

which exactly cancels the pole contributions from $\mathcal{D}$ in Eq. (2). As a result, the only poles present in $\mathcal{M}_3$ are those given by Eq. (B1).

Equation (B1) describes states appearing in the $\mathcal{K}_3 = 0$ limit since the F_3^{∞} function has the same poles as $\mathcal{D}$, i.e., it diverges whenever $E = E_n$. Close to unitarity, by evaluating Eq. (9) numerically, we find that F_3^{∞} becomes a log-periodic function of binding energy, ΔE. Moreover, the sign of the $F_3^{\infty\prime}$s first derivative is constrained below the threshold. These features are shown in Fig. 9. Thus, in the $\mathcal{K}_3 = 0$ case, the bounds states obey the discrete scaling symmetry characteristic of Efimov's phenomenon. As we go to higher a, poles of F_3^{∞} accumulate near the energy threshold, and the energy gap between them becomes increasingly small.

In that region, regardless of its functional form, $\mathcal{K}_3$ is to a good approximation constant;[6] see an orange line in Fig. 9 for an example. Therefore, near the threshold, we recover the Efimov scaling for any model of $\mathcal{K}_3$—an effect ensuring the universality of our result. It also confirms the cutoff independence of this behavior at unitarity since various models of the three-body K matrix are equivalent to differing regularization choices.

[6]Except for instances when it has a pole exactly at the threshold.

APPENDIX C: MATCHING OF POLE RESIDUES AT THE THREE-BODY THRESHOLD

As explained in the main text, by studying the evolution of the trimer poles, we found that the nth resonance on the $+1$ sheet reaches the 3φ threshold at the same value of the two-body scattering length at which the nth bound state emerges on the physical energy plane, and the $(n+1)$th resonance appears on the $+1$ sheet. For instance, for $n = 1$ this occurs around $ma = -8.71$, while for $n = 2$ it occurs around $ma = -203$. Moreover, even though the residues behave in a seemingly unrelated manner away from the $E_{\rm thr}^{(3\varphi)}$, they converge to the same number at the value of ma where the transition between Riemann sheets occurs.

In Fig. 10, we present the numerical evidence of this surprising behavior for the $n = 1$ case. We fix $p = k$ by choosing $\varepsilon_p = \varepsilon_k = 2m^2$, and we compute the residues of the first bound state and the first and second resonances. We normalize them by $\mathcal{M}_2(p)^2$ to cancel enhancement from the two-body rescatterings in the final and initial pairs.

Although we cannot analytically continue the amplitude to the Riemann sheets higher than the first unphysical one, for some values of the scattering length, we see its enhancement above the real axis on the $+1$ sheet. It is reminiscent of the narrow resonant "bump" and suggests the existence of a pole in the lower half-plane of the $+2$ sheet. Working under the assumption that this pole is located near the threshold at $ma = -8.71$, we perform a Breit-Wigner fit to the $\mathcal{D}(p,p)$ amplitude $i\epsilon$ above the real energy axis to extract its position and residue. We use the model,

$$\mathcal{D}(p,p) = -\frac{\Gamma_m^2}{E^2 + i\epsilon - E_m^2} + f(E), \tag{C1}$$

where we again fix $p = k$ such that $\varepsilon_k = \varepsilon_p = 2m^2$. The Γ_m^2 is a complex residue, E_m is the pole position of the modeled trimer, and $f(E)$ is a background quadratic function. We perform several fits, differing by the value of ϵ and the form of $f(E)$. Our model depends, in total, on four real parameters when $f(E) = 0$ up to ten for $f(E) = c_0 + c_1 E + c_3 E^2$, where all c_i are complex numbers. At each ma, we find little

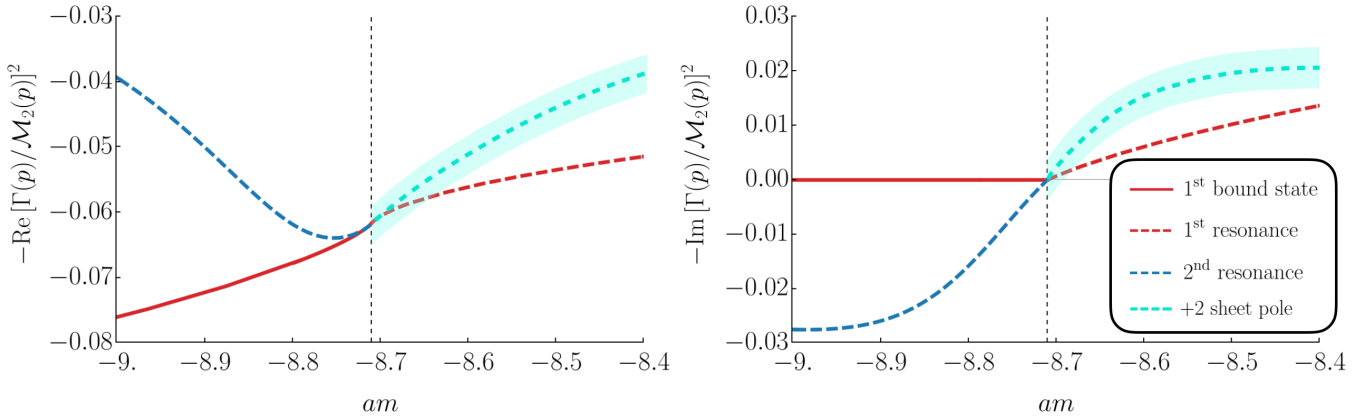

FIG. 10. The *ma* dependence of the normalized trimer residues. Real (left panel) and imaginary (right panel) part of the bound-state residue is shown as a red, solid line. Residues of resonance poles are presented as dashed lines without bands. The first resonance is to the right of the dashed, vertical line, while the second is to the left. The +2 sheet pole, obtained through the extrapolation procedure, is shown with an error band estimate. Around $ma = -8.71$ the poles approach the threshold, and all residues converge to the same value, around -0.061.

variability in values of Γ_m^2 and E_m^2 between different fits, and we take the largest difference between any two of them as the error estimate.

The pole position extracted in this way approaches the three-body threshold as $ma \to -8.71$. In Fig. 10, we also show evidence that the residue of this pole converges to the same value as the residues of the remaining ones, supporting our conjecture about the missing poles. It indicates that the sheet +2 pole is the second Efimov state, as suggested in Fig. 5. However, we note that this result is obtained in an approximate, model-dependent manner and is less reliable than the exact analytic continuation of the amplitude.

[1] V. Efimov, Phys. Lett. B **33**, 563 (1970).
[2] V. Efimov, Nucl. Phys. A **210**, 157 (1973).
[3] K. M. Case, Phys. Rev. **80**, 797 (1950).
[4] V. de Alfaro, S. Fubini, and G. Furlan, Nuovo Cim. A **34**, 569 (1976).
[5] P. Niemann and H. W. Hammer, Few Body Syst. **56**, 869 (2015).
[6] S. M. Dawid, R. Gonsior, J. Kwapisz, K. Serafin, M. Tobolski, and S. D. Głazek, Phys. Lett. B **777**, 260 (2018).
[7] K. G. Wilson, Phys. Rev. D **3**, 1818 (1971).
[8] S. D. Glazek and K. G. Wilson, Phys. Rev. Lett. **89**, 230401 (2002); **92**, 139901(E) (2004).
[9] P. F. Bedaque, H. W. Hammer, and U. van Kolck, Phys. Rev. Lett. **82**, 463 (1999).
[10] H.-W. Hammer and L. Platter, Philos. Trans. R. Soc. London, Ser. A **369**, 2679 (2011).
[11] S. K. Adhikari and L. Tomio, Phys. Rev. C **26**, 83 (1982).
[12] P. F. Bedaque, H. W. Hammer, and U. van Kolck, Nucl. Phys. A **676**, 357 (2000).
[13] E. Garrido, D. V. Fedorov, and A. S. Jensen, Phys. Rev. Lett. **96**, 112501 (2006).
[14] A. Kievsky, M. Gattobigio, L. Girlanda, and M. Viviani, Annu. Rev. Nucl. Part. Sci. **71**, 465 (2021).
[15] E. Braaten and M. Kusunoki, Phys. Rev. D **69**, 074005 (2004).
[16] D. L. Canham, H. W. Hammer, and R. P. Springer, Phys. Rev. D **80**, 014009 (2009).
[17] E. Wilbring, H. W. Hammer, and U.-G. Meißner, arXiv:1705.06176 [hep-ph] (2017).
[18] M. P. Valderrama, Phys. Rev. D **99**, 034010 (2019).
[19] M. P. Valderrama, Phys. Rev. D **98**, 034017 (2018).
[20] T. Kraemer, M. Mark, P. Waldburger, J. G. Danzl, C. Chin, B. Engeser, A. D. Lange, K. Pilch, A. Jaakkola, H.-C. Nägerl, and R. Grimm, Nature (London) **440**, 315 (2006).
[21] M. Zaccanti, B. Deissler, C. D'Errico, M. Fattori, M. Jona-Lasinio, S. Müller, G. Roati, M. Inguscio, and G. Modugno, Nat. Phys. **5**, 586 (2009).
[22] S. E. Pollack, D. Dries, and R. G. Hulet, Science **326**, 1683 (2009).
[23] J. H. Huckans, J. R. Williams, E. L. Hazlett, R. W. Stites, and K. M. O'Hara, Phys. Rev. Lett. **102**, 165302 (2009).
[24] J. R. Williams, E. L. Hazlett, J. H. Huckans, R. W. Stites, Y. Zhang, and K. M. O'Hara, Phys. Rev. Lett. **103**, 130404 (2009).
[25] N. Gross, Z. Shotan, S. Kokkelmans, and L. Khaykovich, Phys. Rev. Lett. **103**, 163202 (2009).
[26] F. Ferlaino, S. Knoop, M. Berninger, W. Harm, J. P. D'Incao, H.-C. Nägerl, and R. Grimm, Phys. Rev. Lett. **102**, 140401 (2009).
[27] T. Lompe, T. B. Ottenstein, F. Serwane, K. Viering, A. N. Wenz, G. Zürn, and S. Jochim, Phys. Rev. Lett. **105**, 103201 (2010).
[28] S. Nakajima, M. Horikoshi, T. Mukaiyama, P. Naidon, and M. Ueda, Phys. Rev. Lett. **105**, 023201 (2010).
[29] N. Gross, Z. Shotan, S. Kokkelmans, and L. Khaykovich, Phys. Rev. Lett. **105**, 103203 (2010).
[30] M. Berninger, A. Zenesini, B. Huang, W. Harm, H.-C. Nägerl, F. Ferlaino, R. Grimm, P. S. Julienne, and J. M. Hutson, Phys. Rev. Lett. **107**, 120401 (2011).
[31] R. J. Wild, P. Makotyn, J. M. Pino, E. A. Cornell, and D. S. Jin, Phys. Rev. Lett. **108**, 145305 (2012).

[32] B. Huang, L. A. Sidorenkov, R. Grimm, and J. M. Hutson, Phys. Rev. Lett. **112**, 190401 (2014).
[33] D. V. Fedorov and A. S. Jensen, Phys. Rev. Lett. **71**, 4103 (1993).
[34] A. Delfino and T. Frederico, Phys. Rev. C **53**, 62 (1996).
[35] G. J. Hanna and D. Blume, Phys. Rev. A **74**, 063604 (2006).
[36] E. Braaten and H. W. Hammer, Phys. Rep. **428**, 259 (2006).
[37] L. Pricoupenko, Phys. Rev. A **82**, 043633 (2010).
[38] J. von Stecher, J. Phys. B **43**, 101002 (2010).
[39] J. Wang, J. P. D'Incao, B. D. Esry, and C. H. Greene, Phys. Rev. Lett. **108**, 263001 (2012).
[40] P. Naidon, S. Endo, and M. Ueda, Phys. Rev. Lett. **112**, 105301 (2014).
[41] Y. Horinouchi and M. Ueda, Phys. Rev. Lett. **114**, 025301 (2015).
[42] P. Naidon and S. Endo, Rep. Prog. Phys. **80**, 056001 (2017).
[43] C. H. Greene, P. Giannakeas, and J. Perez-Rios, Rev. Mod. Phys. **89**, 035006 (2017).
[44] A. Deltuva, Phys. Rev. C **103**, 064001 (2021).
[45] D. S. Rosa, T. Frederico, G. Krein, and M. T. Yamashita, Phys. Rev. A **106**, 023311 (2022).
[46] T. Frederico and M. Gattobigio, Phys. Rev. A **108**, 033302 (2023).
[47] L. Pricoupenko, Phys. Rev. A **108**, 013315 (2023).
[48] M. T. Hansen and S. R. Sharpe, Phys. Rev. D **90**, 116003 (2014).
[49] M. T. Hansen and S. R. Sharpe, Phys. Rev. D **92**, 114509 (2015).
[50] M. Mai, B. Hu, M. Döring, A. Pilloni, and A. Szczepaniak, Eur. Phys. J. A **53**, 177 (2017).
[51] T. D. Blanton and S. R. Sharpe, Phys. Rev. D **102**, 054520 (2020).
[52] R. A. Briceño, M. T. Hansen, and S. R. Sharpe, Phys. Rev. D **95**, 074510 (2017).
[53] R. A. Briceño, M. T. Hansen, and S. R. Sharpe, Phys. Rev. D **99**, 014516 (2019).
[54] M. T. Hansen, F. Romero-López, and S. R. Sharpe, J. High Energy Phys. 07 (2020) 047; 02 (2021) 014(E).
[55] T. D. Blanton and S. R. Sharpe, Phys. Rev. D **104**, 034509 (2021).
[56] T. D. Blanton and S. R. Sharpe, Phys. Rev. D **102**, 054515 (2020).
[57] A. W. Jackura, S. M. Dawid, C. Fernández-Ramírez, V. Mathieu, M. Mikhasenko, A. Pilloni, S. R. Sharpe, and A. P. Szczepaniak, Phys. Rev. D **100**, 034508 (2019).
[58] R. A. Briceño, M. T. Hansen, S. R. Sharpe, and A. P. Szczepaniak, Phys. Rev. D **100**, 054508 (2019).
[59] T. D. Blanton and S. R. Sharpe, Phys. Rev. D **103**, 054503 (2021).
[60] A. W. Jackura, Phys. Rev. D **108**, 034505 (2023).
[61] S. M. Dawid, M. H. E. Islam, and R. A. Briceño, Phys. Rev. D **108**, 034016 (2023).
[62] D. D. Brayshaw, Phys. Rev. **176**, 1855 (1968).
[63] D. D. Brayshaw, Phys. Rev. **167**, 1505 (1968).
[64] W. Glöckle, Phys. Rev. C **18**, 564 (1978).
[65] A. Matsuyama and K. Yazaki, Nucl. Phys. A **534**, 620 (1991).
[66] T. Hyodo, T. Hatsuda, and Y. Nishida, Phys. Rev. C **89**, 032201(R) (2014).
[67] A. Konishi, O. Morimatsu, and S. Yasui, arXiv:1705.02569 [hep-ph].
[68] P. F. Bedaque, H. W. Hammer, and U. van Kolck, Nucl. Phys. A **646**, 444 (1999).
[69] S. Dietz, H.-W. Hammer, S. König, and A. Schwenk, Phys. Rev. C **105**, 064002 (2022).
[70] M. T. Yamashita, T. Frederico, A. Delfino, and L. Tomio, Phys. Rev. A **66**, 052702 (2002).
[71] M. T. Yamashita, T. Frederico, and L. Tomio, Phys. Lett. B **660**, 339 (2008).
[72] M. T. Yamashita, T. Frederico, and L. Tomio, Phys. Rev. Lett. **99**, 269201 (2007).
[73] J. V. Lindesay and H. P. Noyes, SLAC-PUB-2515 (1980).
[74] J. V. Lindesay and H. P. Noyes, SLAC-PUB-2932 (1986).
[75] T. Frederico, Phys. Lett. B **282**, 409 (1992).
[76] J. Carbonell and V. A. Karmanov, Phys. Rev. C **67**, 037001 (2003).
[77] E. Ydrefors, J. H. Alvarenga Nogueira, V. Gigante, T. Frederico, and V. A. Karmanov, Phys. Lett. B **770**, 131 (2017).
[78] E. Ydrefors, J. H. Alvarenga Nogueira, V. A. Karmanov, and T. Frederico, Phys. Lett. B **791**, 276 (2019).
[79] K. Mohseni, A. J. Chaves, D. R. da Costa, T. Frederico, and M. R. Hadizadeh, Phys. Lett. B **823**, 136773 (2021).
[80] T. Frederico and E. Ydrefors, Few Body Syst. **62**, 8 (2021).
[81] A. W. Jackura, R. A. Briceño, S. M. Dawid, M. H. E. Islam, and C. McCarty, Phys. Rev. D **104**, 014507 (2021).
[82] M. T. Hansen, R. A. Briceño, R. G. Edwards, C. E. Thomas, and D. J. Wilson (Hadron Spectrum), Phys. Rev. Lett. **126**, 012001 (2021).
[83] H. Lehmann, K. Symanzik, and W. Zimmermann, Nuovo Cim. **1**, 205 (1955).
[84] W. Zimmermann, Nuovo Cim. **10**, 597 (1958).
[85] Z. Fried, Bound states in the Lehmann, Symanzik and Zimmermann formulation of field theory, Ph.D. thesis, Brandeis University, 1960.
[86] A. Duncan, *The Conceptual Framework of Quantum Field Theory* (Oxford University Press, Oxford, 2012).
[87] L. Landau, Nucl. Phys. **13**, 181 (1959).
[88] R. J. Eden, P. V. Landshoff, D. I. Olive, and J. C. Polkinghorne, *The Analytic S-matrix* (Cambridge University Press, Cambridge, 1966).
[89] H. Burkhardt, *Dispersion Relation Dynamics: A Phenomenological Introduction to S-matrix Theory* (North-Holland, Amsterdam, 1969).
[90] M. T. Hansen and S. R. Sharpe, Phys. Rev. D **95**, 034501 (2017).
[91] R. A. Briceño, M. T. Hansen, and S. R. Sharpe, Phys. Rev. D **98**, 014506 (2018).
[92] See Supplemental Material at http://link.aps.org/supplemental/10.1103/PhysRevA.109.043325. for a video showing the information presented in Fig. 4 of this paper.
[93] F. Bringas, M. T. Yamashita, and T. Frederico, Phys. Rev. A **69**, 040702(R) (2004).
[94] Y. Kamiya and T. Hyodo, Phys. Rev. D **97**, 054019 (2018).
[95] G. S. Adams *et al.* (E852 Collaboration), Phys. Rev. Lett. **81**, 5760 (1998).
[96] M. Aghasyan *et al.* (COMPASS), Phys. Rev. D **98**, 092003 (2018).

[97] L. Antoniazzi *et al.*, Phys. Rev. D **50**, 4258 (1994).
[98] S. K. Choi *et al.* (Belle Collaboration), Phys. Rev. Lett. **91**, 262001 (2003).
[99] R. Aaij *et al.* (LHCb Collaboration), Nat. Phys. **18**, 751 (2022).
[100] R. Aaij *et al.* (LHCb Collaboration), Nat. Commun. **13**, 3351 (2022).
[101] R. Aaij *et al.* (LHCb Collaboration), Phys. Rev. D **90**, 112004 (2014).
[102] H.-Y. Cheng, C.-K. Chua, and Z.-Q. Zhang, Phys. Rev. D **94**, 094015 (2016).
[103] P. Chang, K.-F. Chen, and W.-S. Hou, Prog. Part. Nucl. Phys. **97**, 261 (2017).
[104] R. Aaij *et al.* (LHCb Collaboration), J. High Energy Phys. 07 (2023) 067.
[105] M. T. Hansen and S. R. Sharpe, Phys. Rev. D **93**, 096006 (2016); **96**, 039901(E) (2017).
[106] T. D. Blanton, F. Romero-López, and S. R. Sharpe, J. High Energy Phys. 03 (2019) 106.